

An Automated Cirrus Cloud Detection Method for a Ground-Based Cloud Image

JUN YANG, WEITAO LU, YING MA, AND WEN YAO

Institute of Atmospheric Sounding, Chinese Academy of Meteorological Sciences, Beijing, China

(Manuscript received 30 December 2010, in final form 9 January 2012)

ABSTRACT

Cloud detection is a basic research for achieving cloud-cover state and other cloud characteristics. Because of the influence of sunlight, the brightness of sky background on the ground-based cloud image is usually nonuniform, which increases the difficulty for cirrus cloud detection, and few detection methods perform well for thin cirrus clouds. This paper presents an effective background estimation method to eliminate the influence of variable illumination conditions and proposes a background subtraction adaptive threshold method (BSAT) to detect cirrus clouds in visible images for the small field of view and mixed clear–cloud scenes. The BSAT algorithm consists of red-to-blue band operation, background subtraction, adaptive threshold selection, and binarization. The experimental results show that the BSAT algorithm is robust for all types of cirrus clouds, and the quantitative evaluation results demonstrate that the BSAT algorithm outperforms the fixed threshold (FT) and adaptive threshold (AT) methods in cirrus cloud detection.

1. Introduction

Clouds play an important role in the energy balance of the earth because of their absorption and scattering of solar and infrared radiation (Harshvardhan et al. 1989), and their change is an important influence factor of the global climate (Carslaw et al. 2002). It is very important to monitor clouds, and there are several meteorological satellites providing sky-based large-scale clouds observations around the clock (Hutchison et al. 1995; Jolivet and Feijt 2003; Glantz 2010). Satellite observations have many advantages but suffer from various uncertainties in quantifying cloud features because of their low spatial and temporal resolution (Nordeen et al. 2005). So, ground-based cloud observation is commonly used to improve satellite studies. However, the observation of ground-based cloud mainly depends on visual judgment of the meteorological observers in the past (World Meteorological Organization 2008), which has become a bottleneck of automatic meteorological observation.

With the development of the remote sensing research and digital image processing technology, several ground-based sky-imaging devices are manufactured and applied

to achieve cloud-cover state and other cloud characteristics automatically. Among these instruments, the whole-sky imagers (WSI) (Johnson et al. 1989; Shields et al. 1992), developed by the Scripps Institute of Oceanography at the University of California, San Diego, is the most known. It measures sky radiances at diverse wavelength bands (450, 650, and 800 nm) and acquires the hemisphere sky images, which provides cloud observation results both daytime and nighttime. Another commercially noted instrument is the total-sky image (TSI) (Long and DeLuisi 1998), which was manufactured by the Yankee Environmental Systems, Inc. The TSI provides the hemisphere sky images in visible bands and estimates fractional cloud cover in almost real time of daytime. A number of papers are published using these two noted apparatuses to determine cloud cover and cloud type or classification (Shields et al. 1998; Slater et al. 2001; Long et al. 2006; Sylvio et al. 2010). Some similar functional sky imagers have also been manufactured, such as the whole-sky camera (WSC) (Long et al. 2006; Calbó and Sabburg 2008), developed by the University of Girona in Spain; the all-sky imager (Cazorla et al. 2008), manufactured by Grupo de Física de la Atmósfera (GFAT) at the University of Granada, Spain; and the all-sky images (ASIs) (Huo and Lu 2009), produced by the Key Laboratory for Atmosphere and Global Environment Observation at the Institute of Atmospheric Physics (IAP), Chinese Academy of Sciences.

Corresponding author address: Jun Yang, Institute of Atmospheric Sounding, Chinese Academy of Meteorological Sciences, No. 46 Zhongguancun South Street, Beijing 100081, China.
E-mail: yangjun@cams.cma.gov.cn

Cloud detection is the basis for determining cloud cover and cloud type. Using aforementioned instruments, many cloud detection algorithms were proposed. These algorithms can be categorized into two types: without any a priori knowledge and a priori knowledge based. In the literature, the former type mainly refers to 2D red-to-blue bands threshold methods. A single fixed threshold (FT) to the WSI for opaque clouds was presented by Johnson et al. (1988). Long et al. (2006) classified WSC image pixels with a red-to-blue ratio (R/B) greater than 0.6 as cloudy or else as cloudless. Heinle et al. (2010) used $R - B$ instead of R/B and recommended $R - B = 30$ as an optimal fixed threshold to detect cloud in their preprocessing. Considering the complexity of clouds, a single fixed threshold obviously cannot obtain satisfactory cloud determination result. The TSI algorithm uses variable thresholds depending on the relative position between pixels and the sun (Long et al. 2006). Huo and Lu (2009) extended the fixed threshold method to the ASIs by applying a fast Fourier transform (FFT), symmetrical to obtain different thresholds under low visibility conditions. Yang et al. (2009) presented a method to compute adaptive threshold (AT) for different types of clouds based on histogram maximum between-class variance. Of a priori knowledge-based cloud detection methods, Souza-Echer et al. (2006) adopted a 1D linear segmentation based on saturation attribute to determine clear, cloud, or undefined sky state, but the cutoff thresholds were predefined according to some selected samples. Cazorla et al. (2008) used an optimized neural network classifier and a genetic algorithm to discriminate clear sky and two cloud classes: opaque and thin clouds. Sylvio et al. (2010) used Euclidean geometric distance (EGD) and Bayesian statistics methods in a 3D red-green-blue (RGB) color space to classify the sky and cloud patterns. These methods have got some interesting cloud detection results, but they need many training samples or human-computer interaction before cloud detection, which is not conducive to the automatic observation of cloud. So, 2D red-to-blue bands threshold methods are still widely used to detect cloud in most of ground-based sky-imaging devices.

All these 2D threshold algorithms work quite well for optically thick clouds, but few methods that are published in detail perform well for thin cirrus clouds. Because of the influence of sunlight, the brightness and red/blue ratio of sky background on the ground-based cirrus cloud image are usually nonuniform, which increases the difficulty for cirrus cloud detection. The WSI team developed a thin cloud algorithm, which is discussed in Shields et al. (1992, 1998) and Seiz et al. (2007); examples are discussed in Shields et al. (2007a,b). This thin cloud algorithm is based on first identifying opaque clouds based on either

red/blue or NIR/blue ratios and then dividing the residual ratio pixels by a ratio background that varies with look angle, solar zenith angle, and haze amount. However, details of the algorithm have not yet been published, and the algorithm is also quite complex to use. In this paper, we adopt an effective background estimation method to eliminate the influence of variable illumination conditions and bring up a background subtraction adaptive threshold method (BSAT) to detect cirrus clouds from the ground-based visible cloud images automatically. The cirrus cloud image dataset is described briefly in the next section. In section 3, the BSAT algorithm is introduced in detail. Then, several different types of cirrus cloud images are analyzed to evaluate the validity of the proposed method and a quantitative evaluate method is introduced in section 4. Finally, a summary and suggestions for future research are given in section 5.

2. The cirrus cloud image dataset

The cirrus cloud images using in this paper are selected from a cirrus cloud image dataset. The dataset is composed of 181 images, which are collected from two categories: total-sky images and common camera images. The total-sky images are acquired by ground-based total-sky cloud imager (TCI) (Zhang et al. 2010), which is developed by the Institute of Atmospheric Sounding at the Chinese Academy of Meteorological Sciences. The TCI system consists of three components, an industrial digital camera with a fish-eye lens (view angle is 185°), a sun-block device, and an outside protective box. Different from other cloud imagers, TCI adopts a new sun-block mode: that is, without shelter when the camera is imaging or else sheltering all the view range completely during nonimaging period, which is actualized by automatic opening and closing of a set of spherical vanes. It can provide an RGB color image with a resolution of 1392×1024 pixels every 1 min. A number of total-sky images are collected from June 2009 to October 2010 by three TCI devices, which are located at Beijing (39.8089°N , 116.4719°E), Conghua (23.5679°N , 113.6150°E), and Yangjiang (21.8455°N , 111.9783°E) in China. Figure 1 shows the TCI device and a case of TCI image. The common camera images are shot by the coauthors from different sites at different times. Considering that the areas influenced by the direct sunlight are often overexposure, these areas are not included in the dataset. That is to say, we only analyze the images with a limited field of view. So, the two types of images are viewed by human eyes and some typical cirrus cloud subregions are cropped to form the final cirrus cloud image dataset.



FIG. 1. Ground-based TCI: (left) TCI device and (right) an example of TCI image obtained at 0625 local time (LT) 30 Jun 2010 in Yangjiang, China.

3. Background subtraction adaptive threshold algorithm

In clear sky, sunlight scatters off molecules and other particles much smaller than the wavelength of the light in the atmosphere. The scattering of molecular air is called Rayleigh scattering, which is inversely proportional to the fourth power of wavelength, so that shorter-wavelength violet and blue light will scatter more than the longer red wavelength. Real atmospheres include small particles such as may be characterized by haze. The scattering in these atmospheres is called Mie scattering and results in a proportionality that is less strong than Rayleigh and that depends on how clean and clear the air is. On the other hand, the cloud consists of water droplets that are much larger than the droplets associated with either haze or clear air, and the scattering from them is almost independent of wavelength in the visible spectrum (Nishita et al. 1993). This is the reason why the sky is the blue color against white clouds to our eyes. Almost all the cirrus cloud images are consistent with or similar to meet the rules.

Using this property, many researchers separated clouds from sky background based on the ratio of red-to-blue channel (Shields et al. 1998; Slater et al. 2001; Long et al. 2006; Calbó and Sabburg 2008). The objective of this operation is increasing the differentia between the clear sky and the clouds. Considering that log-ratio operation, difference operation, and normalized difference operation also have similar effects with ratio operation, we compare the mentioned four operations in order to choose a more suitable method for the cirrus cloud detection.

a. Overview of the new algorithm

The proposed cirrus cloud detection method consists of red-to-blue band operation, background subtraction,

adaptive threshold selection, and binarization. The whole flowchart is illustrated as Fig. 2. First, a red-to-blue channel operation is performed to transfer the original RGB image into a single channel image in order to enhance the differentia between the cloud and background. Second, morphology opening operation is used to estimate nonuniform illumination background, and the background subtraction result can be obtained by subtracting the background image from the channel operation result image. Then, a threshold method is used to compute an adaptive threshold for the background subtraction image. Finally, a binarization processing is done to distinguish cloud and sky pixels. The effectiveness of BSAT algorithm is based on the histogram bimodal distribution of images. When the sky is clear or overcast, it is not suitable for using the BSAT algorithm. The related solutions have been mentioned in Li et al. (2011). In this paper, we focus on the detection of cirrus cloud for a limited field of view and a mixed clear/cloud scene. The detailed steps of the BSAT will be explained in the following sections.

b. Four blue-to-red channel operation methods

The equations of ratio, log-ratio, difference, and normalized difference operation are as follows:

$$V_r = R/B, \quad (1)$$

$$V_l = \log(R)/\log(B), \quad (2)$$

$$V_d = R - B, \quad \text{and} \quad (3)$$

$$V_n = \frac{R - B}{R + B}, \quad (4)$$

where R and B represent red and blue channel gray values, respectively, and V_r , V_l , V_d , and V_n are the

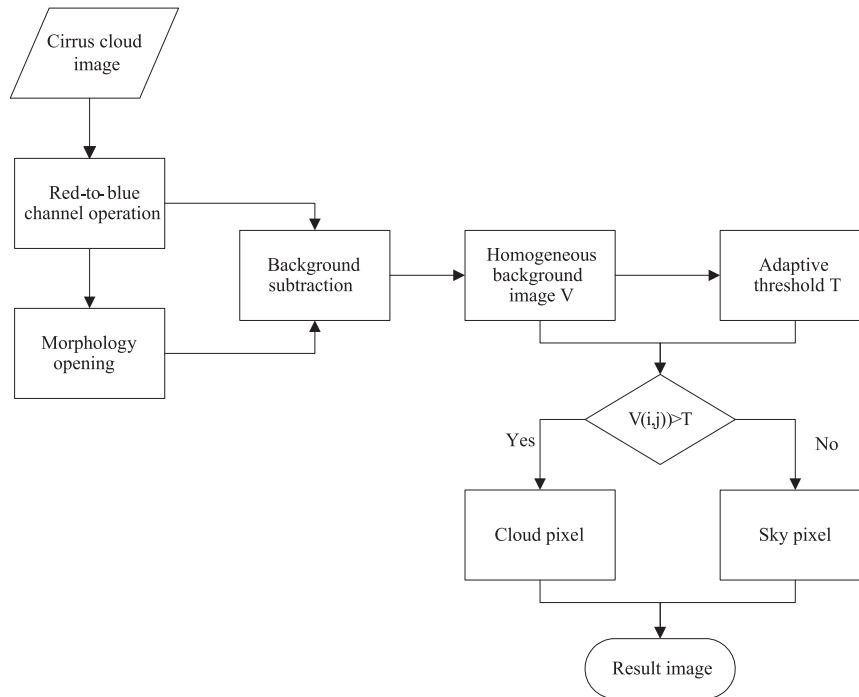


FIG. 2. The flowchart of the proposed cirrus cloud detection.

corresponding results of ratio, log-ratio, difference, and normalized difference operation.

To choose the most appropriate band operation for cirrus cloud image, four operation methods are calculated respectively for 181 cirrus cloud images. These images have similar results, and Fig. 3 shows one of the results. To better display, all images are converted to an unsigned 8-bit format. In Fig. 3, the left panel shows the original image, which is a subregion of Fig. 1; the top panels show the ratio, log-ratio, difference, and normalized difference operation results from left to right in turn; and the bottom panels show the corresponding normalized histograms. From these histograms, it can be found that the gray values are on the high side after ratio and log-ratio operations, and the values are on the low side after difference operation, whereas the operation of normalized difference acquires the biggest grayscale, which will help to improve the detection accuracy of cirrus cloud. So, in the next step, normalized difference operation of red-to-blue band is applied to the original RGB image instead of ratio.

c. Background subtraction

Background subtraction is widely applied in video surveillance system (Piccardi 2004), which is used to detect a movement or significant differences inside of the video frame. In this paper, a mathematical morphology processing is adopted to estimate sky background based on a single cirrus cloud image.

Mathematical morphology is a nonlinear theory for image processing based on set and lattice theory. It was originally developed for binary images, and it was later extended to grayscale images. Dilation and erosion are two elementary morphology operations (Gonzalez et al. 2004). Mathematically, the dilation of set A (which in this case is a cloud image) by E is defined as

$$A \oplus E = [z | (\hat{E})_z \cap A \neq \phi], \quad (5)$$

where $A \oplus E$ is the result of dilation, z is an element of A , E is the structuring element, \hat{E} means the reflection of E , $(\hat{E})_z$ denotes the translation of set \hat{E} by z , \cap represents the intersection of two sets, and ϕ is the empty set. The definition of erosion is similar to that of dilation. The erosion of set A by E , which is denoted as $A \ominus E$, is defined as

$$A \ominus E = [z | (E)_z \cap A^c \neq \phi], \quad (6)$$

where $(E)_z$ is the translation of set E by z and A^c is the complement of set A .

In image processing domain, dilation and erosion are used most often in various combinations. Opening and closing operations are two best common combinations of dilation and erosion. The morphological opening of A by E , which is denoted as $A \circ E$, is simply erosion of A by E , followed by dilation of the result by E ,

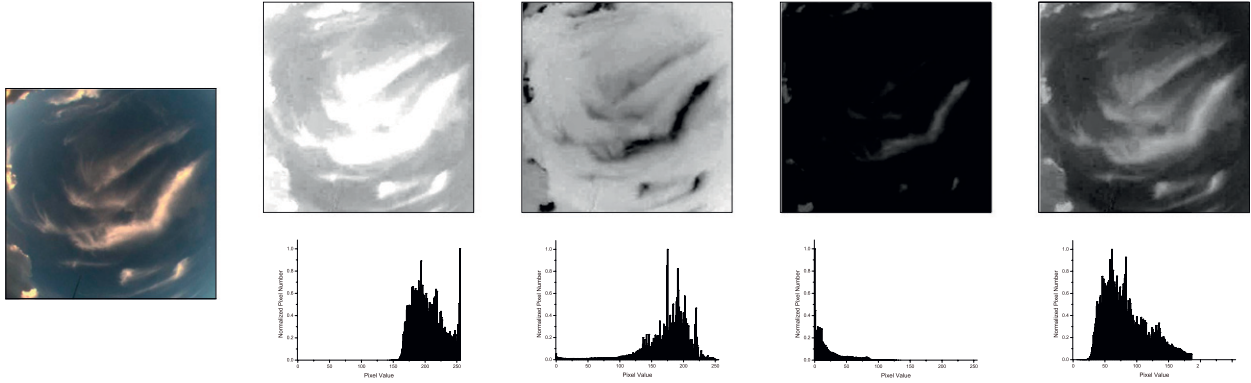


FIG. 3. Comparison of the four channel operation methods: (far left) original image; (top, left to right) ratio, log-ratio, difference, and normalized difference operation results; and (bottom) the corresponding normalized histograms.

$$A \circ E = (A \ominus E) \oplus E. \tag{7}$$

The closing operation of A by E , which is denoted as $A \bullet E$, is a dilation followed by an erosion,

$$A \bullet E = (A \oplus E) \ominus E. \tag{8}$$

Opening operation can be used to estimate background for nonuniform illumination conditions. According to the definition of opening, the structure element is prerequisite. Structure element has all kinds of shapes, including line, disk, diamond, rectangle, square, and so on. Considering cirrus clouds are often wispy or in ripples arranged in a regular formation, a flat, rectangle-shaped structuring element is adopted in this paper, and two nonnegative integers are needed to specify the size of rectangle.

To estimate background accurately, the size of the structure element should be larger than the cirrus clouds. Figure 4 shows an example of background subtraction with structure elements of different sizes. The left panel is the original image with a nonuniform illumination background. When the structure size is smaller than the big rectangle in the center of the image, the background (top left panel) can be estimated partly, but the middle rectangle is misestimated as background. Then subtracting the background image from the original image, the background subtraction result (top middle panel) can be obtained. The top-right image shows the ultimate binarization result. When the structure size is bigger than the middle rectangle, the estimated background is well. All the objects are detected correctly. The corresponding results are shown in the bottom panels of Fig. 4.

d. Adaptive threshold and binarization

After background subtraction, the cloud pixels can be marked as foreground against sky background. The histogram represents the brightness values as a bimodal

distribution. The Otsu (1979) threshold method can be used to choose an adaptive threshold by maximizing between-class variance of the two types. The basic idea of Otsu is as follows:

Suppose the gray levels of the given image can be represented as L . The number of pixels at level i is denoted by n_i and the total number of pixels is denoted by $N = \sum_{i=1}^L n_i$. The probability of each gray value is represented as $P_i = n_i/N$. If the pixels of the image are divided into two class C_B and C_O (background and object, which in this case is clouds) by a threshold at level T , then the probabilities of each class are given as

$$\omega_B = \frac{\sum_{i=1}^T n_i}{N} = \sum_{i=1}^T P_i \quad \text{and} \tag{9}$$

$$\omega_O = \frac{\sum_{i=T+1}^L n_i}{N} = \sum_{i=T+1}^L P_i = 1 - \omega_B, \tag{10}$$

respectively. The average gray values of the classes can be denoted as

$$\mu_B = \frac{\sum_{i=1}^T n_i \times i}{\sum_{i=1}^T n_i} = \frac{\sum_{i=1}^T P_i \times i}{\omega_B} \quad \text{and} \tag{11}$$

$$\mu_O = \frac{\sum_{i=T+1}^L n_i \times i}{\sum_{i=T+1}^L n_i} = \frac{\sum_{i=T+1}^L P_i \times i}{\omega_O}, \tag{12}$$

whereas the total average gray of the original image can be represented as

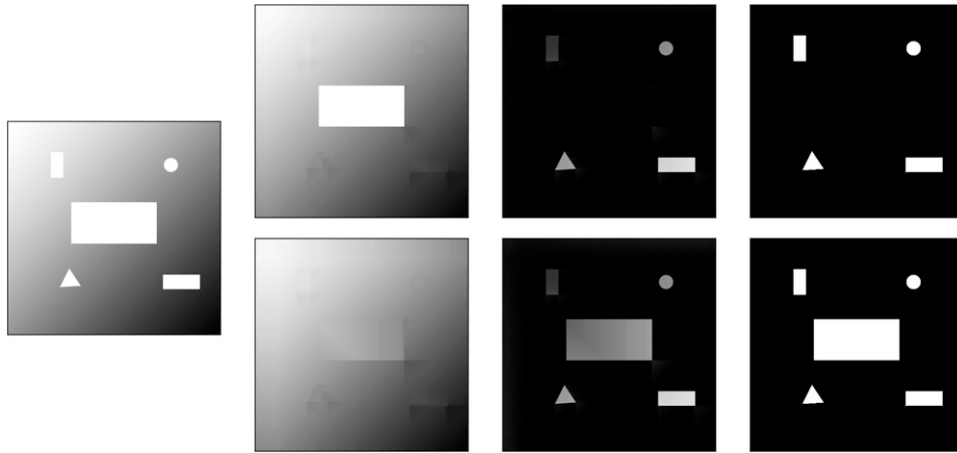


FIG. 4. Examples of background subtraction with structure element of different sizes: (far left) the original images; (top, left to right) results of the opening operation, background subtraction, and binarization with a small structure element; and (bottom) the corresponding results with an big structure element.

$$\begin{aligned}\mu &= \sum_{i=1}^L P_i \times i = \sum_{i=1}^T P_i \times i + \sum_{i=T+1}^L P_i \times i \\ &= \mu_B \omega_B + \mu_O \omega_O.\end{aligned}\quad (13)$$

The between-class variance between background and object is

$$\begin{aligned}\sigma^2(T) &= \omega_B(\mu_B - \mu)^2 + \omega_O(\mu_O - \mu)^2 \\ &= \omega_B \omega_O (\mu_B - \mu_O)^2.\end{aligned}\quad (14)$$

The threshold T , which maximizes $\sigma^2(T)$, is the optimal threshold to segmentation object and background. Using this adaptive threshold, the background subtraction result can be divided into two classes. The pixels whose gray values are larger than threshold T are labeled as clouds or else are labeled as cloudless.

4. Experimental results and accuracy evaluation

To illustrate the performance of the proposed method, five different types of cirrus cloud images, which are named C1, C2, C3, C4, and C5, are taken as examples from the cirrus cloud image dataset in this paper. Figure 5 shows the experimental results of the proposed method. The size of the rectangle-shaped structuring element is 200×200 . C1, C2, C3, C4, and C5 are displayed from top to bottom in turn. The left column is the original images. The second and third columns are the steps in order to get the result images (right column). By visual examination, the results of the red-to-blue channel normalized difference (second column) have obvious nonuniform background brightness, and the

background and cloud are interacting with each other in many regions. After background subtraction, the clouds have clear boundaries and the backgrounds have homogeneous brightness (third column). In the BSAT result images, white represents clouds and black denotes sky regions. Comparing the BSAT results with the original images, the cirrus cloud detection effects are satisfactory.

Another five different type cirrus cloud images, which are denoted as C6, C7, C8, C9, and C10, are used to further evaluate the good performance of the BSAT algorithm. In this paper, the BAST results are compared with the two alternate methods, the FT algorithm and the AT algorithm. The results are not compared with the WSI thin cloud algorithm, because the details of how to apply the WSI algorithm are not readily available. Here, the fixed threshold $R/B = 0.6$ (Long et al. 2006) is adopted in the FT algorithm. The method of Yang et al. (2009) is adopted in the AT algorithm. Figure 6 shows the experimental results of the three methods. C6, C7, C8, C9, and C10 are displayed from top to bottom in turn, where the left images are the original images, the middle-left images are the FT results, the middle-right images are the AT results, and the right images are the results of the proposed BSAT.

By human examination, the FT results failure to distinguish some cirrus clouds in C7, C8, and C9 obviously, whereas the AT results misclassify some sky regions as clouds in the same images. Both the FT and AT methods undetected some thin cirrus clouds for C6 but identify many sky regions as clouds for C10. The proposed BSAT obtains satisfactory visual effects for all the five images.

In addition to visual evaluation, a good quantitative evaluation method is necessary. Cloud detection is

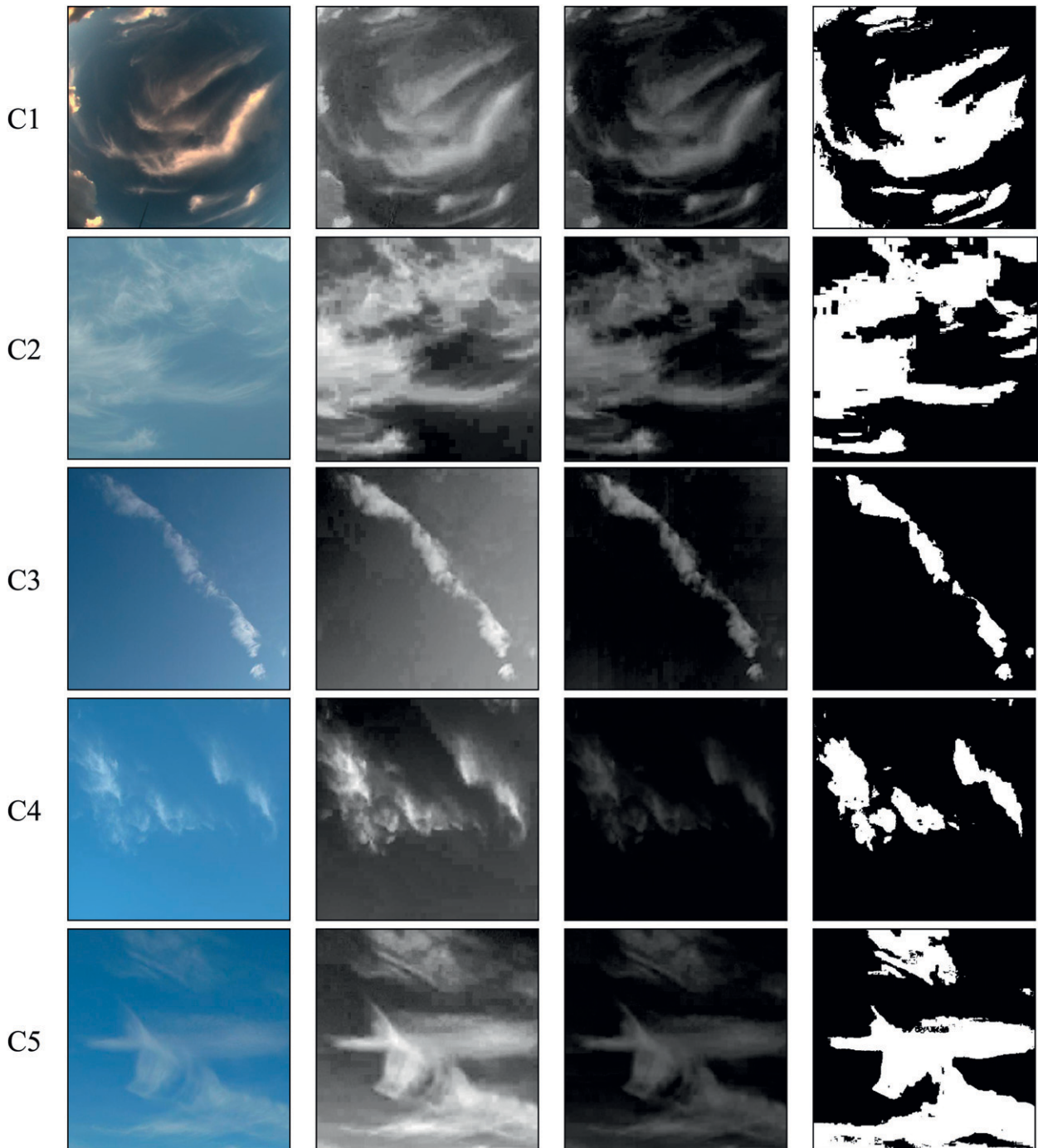


FIG. 5. Experimental results of the BSAT algorithm: (left) the original images, (middle left) results of the blue-to-red channel normalized difference, (middle right) results of the background subtraction, and (right) results of the BSAT.

actually a binary classification, and there are four possible categories for each pixel:

True positive (TP): Both the visual and the detection method classify the pixel as cloud.

True negative (TN): Both the visual and the detection method classify the pixel as sky.

False positive (FP): The visual classifies the pixel as sky, but the detection method classifies the pixel as cloud.

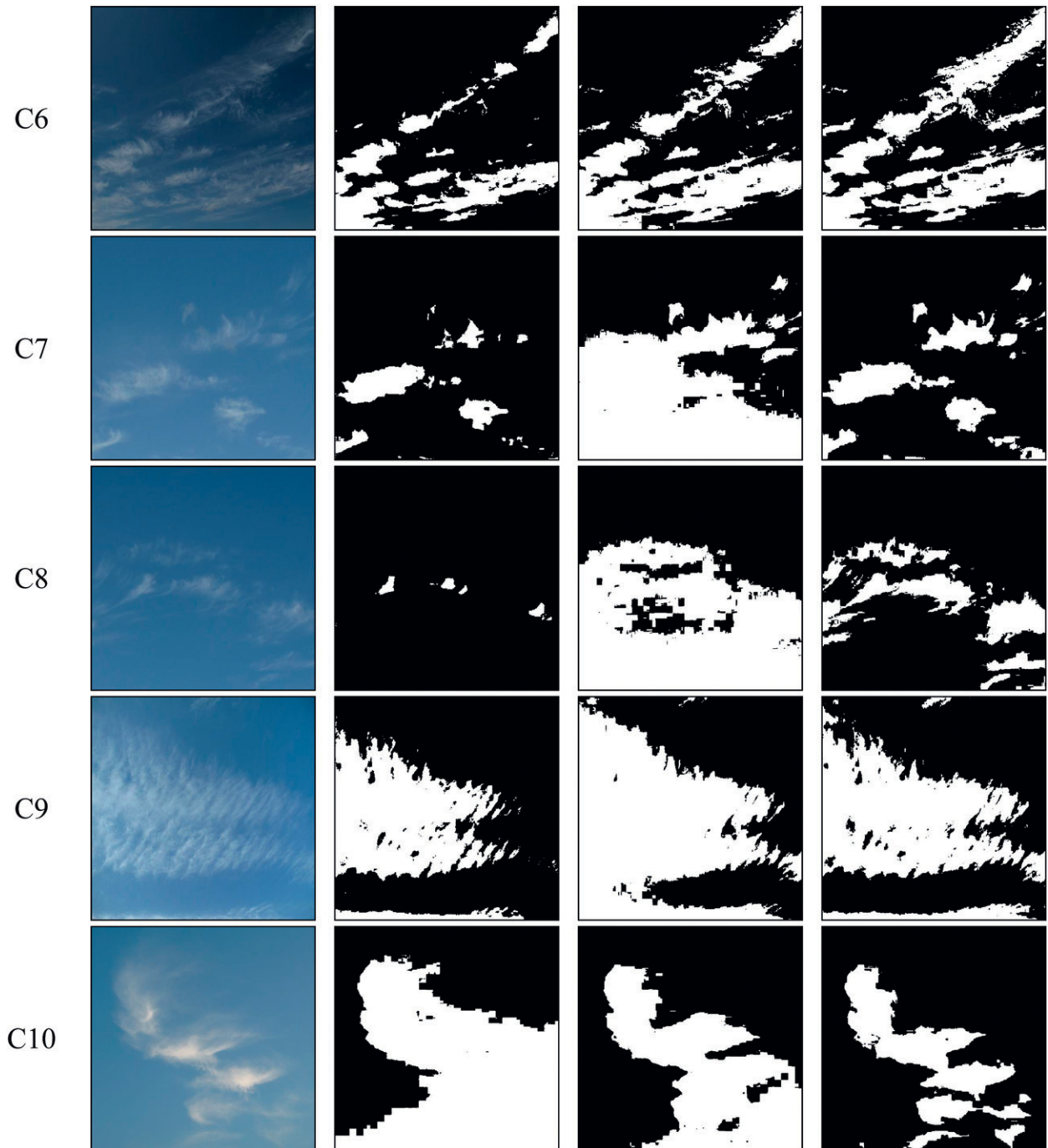


FIG. 6. Experimental results of the three methods: (left) the original images, (middle left) results of the FT, (middle right) results of the AT, and (right) results of the BSAT.

False negative (FN): The visual classifies the pixel as cloud, but the detection method classifies the pixel as sky.

A similar method has been adopted by Shufelt (1999) for building detection evaluation. Here, we use the following two indexes for cirrus cloud detection assessment:

correctness: $TP/(TP + FN)$ and
accuracy: $TP/(TP + FP + FN)$.

The correctness is a measure of the correctly detected cloud pixels among all the cloud pixels. The accuracy reports the total accuracy of the method, which takes both FP and FN into account. For a good cloud

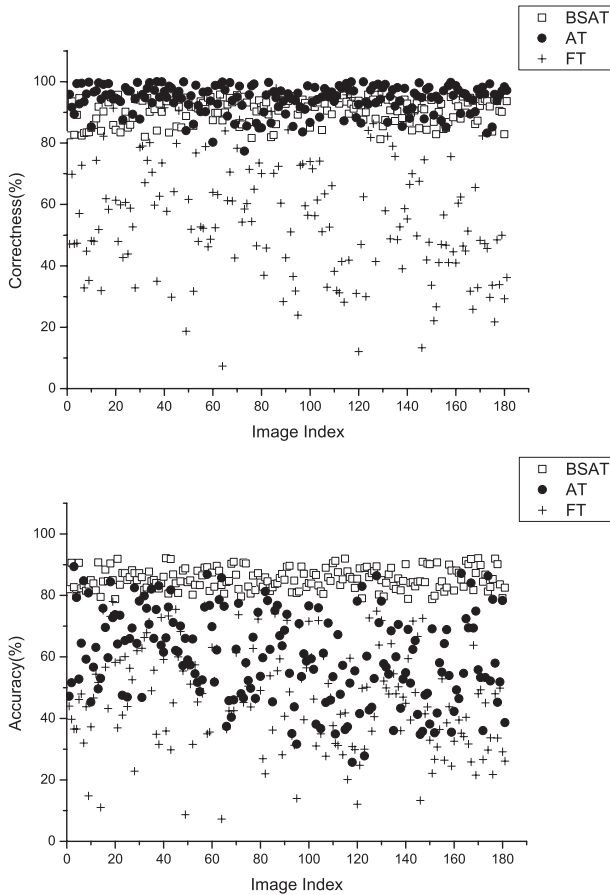


FIG. 7. Quantitative evaluation results on the dataset for the three methods: (top) correctness of the three methods and (bottom) accuracy of the three methods.

detection algorithm, both correctness and accuracy should be higher. To compute these two indexes, a series of standard cloud masks are manually interpreted by an experienced cloud observer as the cloud truth classification.

Figure 7 shows the quantitative evaluation results of the three methods to the whole dataset. Both the correctness and accuracy of the FT algorithm are almost the lowest in the three methods. The AT method obtains the highest correctness for the most test images, but the accuracy are obvious lower than the BSAT, which means the AT algorithm misclassifies many clear-sky pixels as

clouds, whereas the correctness of the BSAT is close to the AT method and the accuracy is the highest. The statistical results (maximum, minimum, and average) of the three methods can be found in Table 1, which denotes the BSAT algorithm outperforms the FT and AT methods in cirrus cloud detection. The average detection correctness of the BSAT is 90.45%, and the accuracy is 85.38%.

The BSAT algorithm is proposed for detecting cirrus cloud in a limited view. We did a preliminary test of the performance of the BSAT for all-sky images. Three TCI images, which are named C11, C12, and C13, are analyzed to test the BSAT. Figure 8 shows the experimental results. C11, C12, and C13 are displayed from top to bottom in turn. The middle-left images are the results of the red-to-blue channel normalized difference. Results after background subtraction are shown in the middle-right images. Comparing the BSAT results (the right images) with the original images (the left images), the cloud detection effects for TCI images are satisfactory, but the regions near the sun and the horizon still have some misclassification.

5. Conclusions

Automatic cloud observation is an urgent task for meteorological stations. Many ground-based cloud devices (WSI, TSI, WSC, ASIs, and TCI) are manufactured with the aim of solving this problem. Cloud detection is a basic research for achieving cloud-cover state and other cloud characteristics. The FT and AT algorithms, which are two alternate 2D red-to-blue bands threshold methods, are widely used in these instruments to detect cloud automatically. They work quite well for optically thick clouds, but few methods perform well for thin cirrus clouds. In this paper, we propose a background subtraction adaptive threshold method to detect cirrus clouds from the ground-based visible cloud images automatically. The experimental results show that the BSAT algorithm is robust for all types of cirrus clouds for the small field of view and mixed clear–cloud scenes we have tested. The quantitative evaluation results demonstrate that the BSAT algorithm outperforms the FT and AT methods in cirrus cloud detection for these test scenarios. It must be noted that, although the BSAT

TABLE 1. Quantitative evaluation results of the three methods.

	FT			AT			BSAT		
	Min	Max	Mean	Min	Max	Mean	Min	Max	Mean
Correctness (%)	7.34	99.91	57.75	77.35	99.98	94.20	81.27	95.81	90.45
Accuracy (%)	7.26	78.98	46.62	25.70	89.35	60.07	78.76	92.06	85.38

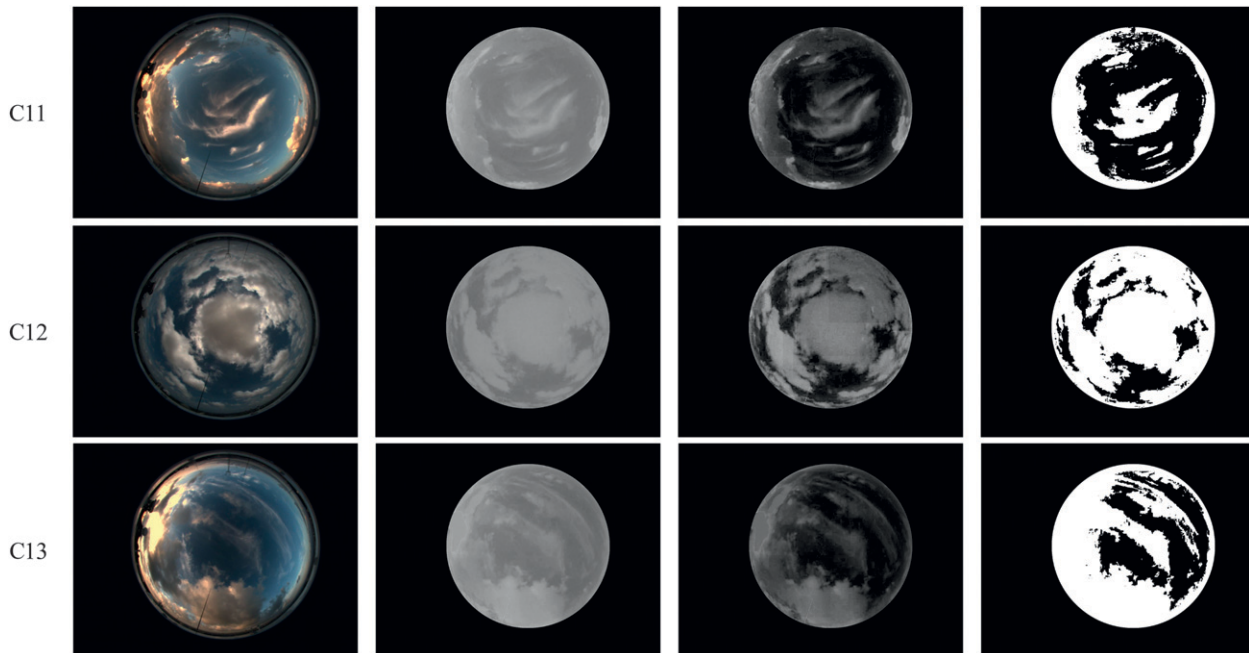


FIG. 8. Experimental results of the BSAT algorithm to TCI images: (left) the original images, (middle left) results of the blue-to-red channel normalized difference, (middle right) results of the background subtraction, and (right) results of the BSAT.

algorithm is proposed for detecting cirrus cloud, it still can be extended to deal with the more general all-sky images. There are several problems need to be solved. The first problem is how to identify the image is clear, overcast, or mixed automatically. The related solutions have been mentioned in Li et al. (2011), which identified the image as unimodal or bimodal distribution according to its standard deviation. The second problem is how to estimate background in a complex all-sky image. A big structure element or multimorphological processing is the optional solution for background estimation. The third problem is the impact of direct sunlight, because the area influenced by the direct sunlight is often overexposure, which may not be removed by background subtraction. So, the overexposure region can be considered as clouds in the first step of cloud detection. Then, in the second step, the specific location of the sun in the image can be calculated by using the longitude, latitude, and time of the image. Using its property of high brightness, the area of sun can be identified accurately. Finally, the result of the first step is subtracted from the second step, which yields the desired cloud detection result.

Acknowledgments. The authors acknowledge the support from the National Natural Science Foundation of China (Grant 41105121), the Basic Research Fund of Chinese Academy of Meteorological Sciences (Grant

2011Z002), and Special Technical D&R Project for Scientific Academies or Institutes of China (Grant NCSTE-2006-JKZX-303). They thank the anonymous reviewers for their constructive comments.

REFERENCES

- Calbó, J., and J. Sabburg, 2008: Feature extraction from whole-sky ground-based images for cloud-type recognition. *J. Atmos. Oceanic Technol.*, **25**, 3–14.
- Carlsaw, K. S., R. G. Harrison, and J. Kirkby, 2002: Cosmic rays, clouds, and climate. *Science*, **298**, 1732–1737.
- Cazorla, A., J. Olmo, and L. Alados-Arboledas, 2008: Development of a sky imager for cloud cover assessment. *J. Opt. Soc. Amer.*, **25A**, 29–39.
- Glantz, P., 2010: Satellite retrieved optical thickness sensitive to surface wind speed in the subarctic marine boundary layer. *Environ. Res. Lett.*, **5**, 034002 doi:10.1088/1748-9326/5/3/034002.
- Gonzalez, R. C., R. E. Woods, and S. L. Eddins, 2004: *Digital Image Processing Using MATLAB*. Pearson Prentice Hall, 609 pp.
- Harshvardhan, D. A. Randall, T. G. Corsetti and D. A. Dazlich, 1989: Earth radiation budget and cloudiness simulations with a general circulation model. *J. Atmos. Sci.*, **46**, 1922–1942.
- Heinle, A., A. Macke, and A. Srivastav, 2010: Automatic cloud classification of whole sky images. *Atmos. Meas. Tech.*, **3**, 557–567.
- Huo, J., and D. Lu, 2009: Cloud determination of all-sky images under low-visibility conditions. *J. Atmos. Oceanic Technol.*, **26**, 2172–2181.
- Hutchison, K. D., K. R. Hardy, and B. C. Gao, 1995: Improved detection of optically thin cirrus clouds in nighttime multispectral

- meteorological satellite using total integrated water vapor information. *J. Appl. Meteor.*, **34**, 1161–1168.
- Johnson, R. W., T. L. Koehler, and J. E. Shields, 1988: A multi-station set of whole sky imagers and a preliminary assessment of the emerging data base. *Proc. Cloud Impacts on DOD Operations and Systems Workshop*, Silver Spring, MD, Department of Defense, 159–162.
- , W. S. Hering, and J. E. Shields, 1989: Automated visibility and cloud cover measurements with a solid-state imaging system. Scripps Institution of Oceanography Marine Physical Laboratory Final Rep. 89-7, 127 pp.
- Jolivet, D., and A. J. Feijt, 2003: Cloud thermodynamic phase and particle size estimation using the 0.67 and 1.6 μm channels from meteorological satellites. *Atmos. Chem. Phys. Discuss.*, **3**, 4461–4488.
- Li, Q., W. Lu, and J. Yang, 2011: A hybrid thresholding algorithm for cloud detection on ground-based color images. *J. Atmos. Oceanic Technol.*, **28**, 1286–1296.
- Long, C. N., and J. J. DeLuise, 1998: Development of an automated hemispheric sky imager for cloud fraction retrievals. *Proc. 10th Symp. on Meteorological Observations and Instrumentation*, Phoenix, AZ, Amer. Meteor. Soc., 171–174.
- , J. M. Sabburg, J. Calbó, and D. Pagès, 2006: Retrieving cloud characteristics from ground-based daytime color all-sky images. *J. Atmos. Oceanic Technol.*, **23**, 633–652.
- Nishita, T., T. Sirai, K. Tadamura, and E. Nakamae, 1993: Display of the earth taking into account atmospheric scattering. *Proc. SIGGRAPH 93*, Anaheim, CA, Association for Computing Machinery, 175–182.
- Nordeen, M. L., M. M. Khaiyer, D. R. Doeling, and D. Phan, 2005: Comparison of surface and satellite-derived cloud and radiation properties at the atmospheric radiation measurement Southern Great Plains and tropical western Pacific. *Proc. 15th ARM Science Team Meeting*, Daytona, FL, NASA, 14 pp.
- Otsu, N., 1979: A threshold selection method from gray level histograms. *IEEE Trans. Syst. Man Cybern.*, **9**, 62–66.
- Piccardi, M., 2004: Background subtraction techniques: A review. *Proc. Int. Conf. on Systems, Man and Cybernetics*, Hague, Netherlands, IEEE, Vol. 4, 3099–3104.
- Seiz, G., J. Shields, U. Feister, E. P. Baltsavias, and A. Gruen, 2007: Cloud mapping with ground-based photogrammetric cameras. *Int. J. Remote Sens.*, **28**, 2001–2032.
- Shields, J. E., R. W. Johnson, and M. E. Karr, 1992: An automated observing system for passive evaluation of cloud cover and visibility. Scripps Institution of Oceanography Marine Physical Laboratory Rep. SIO 92-22, 39 pp.
- , —, —, and J. L. Wertz, 1998: Automated day/night whole sky imagers for field assessment of cloud cover distribution and radiances distributions. *Proc. 10th Symp. on Meteorological Observation and Instrumentation*, Phoenix, AZ, Amer. Meteor. Soc., 165–170.
- , M. E. Karr, A. R. Burden, R. W. Johnson, and W. S. Hodgkiss, 2007a: Whole sky imaging of clouds in the visible and IR for starfire optical range. Scripps Institution of Oceanography Marine Physical Laboratory Tech. Note 272, 67 pp.
- , —, —, —, and —, 2007b: Continuing support of cloud free line of sight determination, including whole sky imaging of clouds. Scripps Institution of Oceanography Marine Physical Laboratory Tech. Note 273, 60 pp.
- Shufelt, J. A., 1999: Performance evaluation and analysis of monocular building extraction from aerial imagery. *IEEE Trans. Pattern Anal. Mach. Intell.*, **21**, 311–326.
- Slater, D. W., C. N. Long, and T. P. Tooman, 2001: Total sky imager/whole sky imager cloud fraction comparison. *Proc. 11th ARM Science Team Meeting*, Atlanta, GA, NASA, 1–11.
- Souza-Echer, M. P., E. B. Pereira, L. S. Bins, and M. A. R. Andrade, 2006: A simple method for the assessment of the cloud cover state in high-latitude regions by a ground-based digital camera. *J. Atmos. Oceanic Technol.*, **23**, 437–447.
- Sylvio, L. M. N., A. V. Wangenheim, E. B. Pereira, and E. Comunello, 2010: The use of Euclidean geometric distance on RGB color space for the classification of sky and cloud patterns. *J. Atmos. Oceanic Technol.*, **27**, 1504–1517.
- World Meteorological Organization, 2008: Guide to meteorological instruments and methods of observation. 7th ed. WMO Note 8, 681 pp.
- Yang, J., W. Lu, Y. Ma, W. Yao, and Q. Li, 2009: An automatic ground-based cloud detection method based on adaptive threshold (in Chinese). *J. Appl. Meteor. Sci.*, **20**, 713–721.
- Zhang, Y., W. Lu, Y. Ma, W. Yao, and J. Yang, 2010: Ground-based total-sky cloud imager (TCI) based on light-shelter scheme using rotating spherical-vanes (in Chinese). Chinese Utility Model Patent ZL200920277594.5, 9 pp.